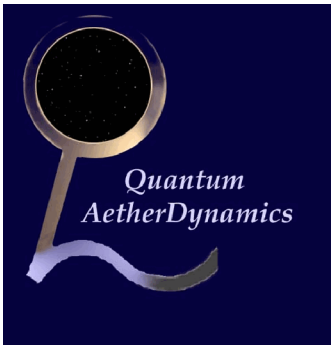

Quantum AetherDynamics Institute (QADI)

Thermoresonant Structural Registration in Photoexcited Tellurium

A QMU Reconstruction of the Dynamic Magneto-Chiral Compatibility Spectrum

David W. Thomson III
Quantum AetherDynamics Institute (QADI), Alma, Illinois, USA
ORCID: 0000-0002-5830-5427
DOI: 10.5281/zenodo.21383938

Version 1.0 – July 15, 2026

This article is published by the Quantum AetherDynamics Institute (QADI).

It develops the Aether Physics Model (APM)

Abstract

A public time-domain terahertz-emission dataset for photoexcited chiral tellurium contains discrete oscillatory modes whose amplitudes grow or decay according to magnetic-field orientation and temperature. This paper reconstructs the deposited oscillator parameters in Quantum Measurement Units and tests whether the transverse amplified spectrum exhibits a direct correspondence with the geometry of trigonal tellurium. QMU temperature is written as temp = area rson, frequency as a fraction of freq = F_q, and the resulting effective thermoresonant cross-section length is

$$L_n(T) = \lambda_C \frac{\sqrt{T/\mathrm{temp}}}{f_n/\mathrm{freq}}.$$

At the measured temperature corresponding to 42 K in the SI bridge, the three deposited transverse branches yield effective lengths of approximately 0.3423, 0.2850, and 0.2191 nm. These register respectively with the interchain Te–Te separation, the intrachain Te–Te bond, and one-half of the transverse lattice parameter. The collective logarithmic registration error is $\mathcal{E}_{\mathrm{reg}} = 0.015791$, corresponding to a root-mean-square fractional mismatch of 1.5646%. An exhaustive comparison of all 210 ordered assignments drawn from seven predefined tellurium dimensions identifies this assignment as the unique optimum at that temperature. A deterministic sensitivity analysis further shows that the optimum assignment survives all independently bounded perturbations of the three deposited frequencies below approximately 22.5 GHz within the predefined candidate set. A scale-independent ratio test, which does not depend on the Kelvin-to-temp conversion factor, agrees at the 2.2–2.6% level. The same assignment is not optimal at the other deposited temperatures, establishing the result as a localized thermoresonant compatibility window rather than a permanent branch identity. The analysis therefore supports a specific and falsifiable hypothesis: the transverse magneto-chiral spectrum enters a thermoresonant compatibility window near $T_{\mathrm{reg}} \approx 42.9$ K, within which three independent resonant pathways simultaneously register with the fixed crystal geometry.

Keywords: Aether Physics Model; Quantum Measurement Units; tellurium; magneto-chiral instability; terahertz emission; structural registration; compatibility spectrum; chiral geometry

1 Introduction

Elemental tellurium is a structurally chiral solid composed of helical atomic chains. Recent time-domain terahertz-emission measurements revealed field-antisymmetric coherent modes that can increase in amplitude after photoexcitation rather than decay monotonically [Huang et al., 2026]. The deposited dataset includes raw time-domain traces, fitted oscillator parameters, field scans, temperature scans, two magnetic-field orientations, and circular-pump controls [Huang and Abboud, 2025]. This unusually complete archive permits the measured response to be studied as a problem of geometric organization rather than only through a prescribed microscopic interpretation.

The primary observable is a family of coherent oscillations characterized by frequency, phase, amplitude, and exponential growth or decay. The deposited fitting convention is

$$E_n(t) = C_n \cos(2\pi f_n t + \phi_n) \exp(-2\pi\gamma_n t)\,.$$

Consequently,

$$\gamma_n < 0 \quad \Longrightarrow \quad \text{amplification},$$

whereas

$$\gamma_n > 0 \quad \Longrightarrow \quad \text{decay}.$$

The experiment therefore provides a measured compatibility landscape: some resonant pathways become constructive under a given orientation and temperature, while others remain dissipative.

The Aether Physics Model interprets temperature, resonance, area, angular orientation, and magnetic organization as physically connected quantities. The QMU thermal identity is

$$\text{temp} = \text{area}\,\text{rson},$$

with

$$\text{area} = {\lambda_C}^2, \qquad \text{rson} = {F_q}^2, \qquad \text{temp} = {\lambda_C}^2 {F_q}^2 = c^2.$$

This relation permits a measured temperature and resonant frequency to be combined into an effective area and length without introducing an arbitrary dimensional constant [Thomson III, 2024, 2025c].

The present paper asks a narrow and testable question: does the deposited tellurium spectrum admit a unique minimum-error assignment to fixed dimensions of the trigonal crystal when the measured temperature and resonance are expressed through the QMU ledger?

The analysis separates three levels of result. First, it identifies an objective numerical property of the deposited spectrum: an optimal ordered mapping between three measured branches and three fixed structural dimensions. Second, it examines whether that mapping represents a coherent geometric organization of the tellurium lattice. Third, it interprets the localized registration condition within the Aether Physics Model as a constructive compatibility state.

The numerical assignment is evaluated before the physical interpretation is applied. The proposed mapping is tested at every deposited transverse temperature, against every ordered assignment drawn from the predefined structural candidate set, and through a second frequency-ratio test that is independent of the absolute Kelvin-to-temp conversion.

2 Experimental Data and Reproducibility

2.1 Deposited archive

The Illinois Data Bank archive contains five experimental groups [Huang and Abboud, 2025]:

1. $B \parallel c$, linear pump, field dependence;
2. $B \parallel c$, linear pump, temperature dependence;
3. $B \perp c$, linear pump, field dependence;
4. $B \perp c$, linear pump, temperature dependence;
5. $B \parallel c$, left- and right-circular pump, field dependence.

Each group includes raw time-domain data, fitted oscillator parameters, and MATLAB scripts used to reproduce the published figures. The data are released under CC BY 4.0 and the deposited code under the MIT License. The present analysis reads the fitted parameter files directly and does not digitize plotted figures.

2.2 Branch definitions

For the transverse-temperature series, the authors' own plotting script identifies modes 4–6 as the three relevant amplified branches. These are labeled here as

$$\text{low}, \qquad \text{core}, \qquad \text{high}.$$

No branch was selected by optimizing the QMU result. The branch indices are inherited from the deposited analysis.

2.3 Structural assignment problem

Let the ordered measured spectrum be

$$\mathcal{F}(T) = \left(f_{\text{low}}(T), f_{\text{core}}(T), f_{\text{high}}(T)\right),$$

and let

$$\mathcal{L} = \{L_1, L_2, \ldots, L_7\}$$

be the predefined set of candidate tellurium structural dimensions.

An ordered structural assignment is a one-to-one mapping

$$\Phi : \mathcal{F}(T) \longrightarrow (L_i, L_j, L_k), \qquad i \neq j \neq k.$$

Because seven candidate dimensions are available for three ordered branches, the complete search contains

$$7 \times 6 \times 5 = 210$$

possible assignments.

The numerical task is therefore not a search for a correlation coefficient. It is a finite assignment problem:

$$\Phi_{\min}(T) = \arg\min_{\Phi} \mathcal{E}_{\text{reg}}(T; \Phi).$$

This terminology is used throughout the paper. The phrase *optimal structural assignment* refers to the mapping that minimizes the registration error over the complete predefined search space.

2.4 Reproducibility package

The accompanying analysis package contains:

- all deposited transverse-temperature oscillator parameters;
- the complete QMU structural-registration table;
- the exhaustive table of all 210 ordered structural assignments;
- assignment rankings at every measured temperature;
- the scale-independent frequency-ratio test;
- all figures used in this paper; and

- a standalone Python reproduction script.

The script performs exact transformations of the deposited best-fit values. The oscillator parameter files do not include covariance matrices or parameter uncertainties. Accordingly, the results are reproducible numerical registrations, not uncertainty-propagated confidence intervals.

3 Tellurium Geometry

Trigonal tellurium consists of helical chains parallel to the crystallographic c-axis. Structural studies report an intrachain Te–Te bond length near

$$d_{\mathrm{intra}} = 0.2835 \text{ nm},$$

an interchain Te–Te separation near

$$d_{\mathrm{inter}} = 0.3495 \text{ nm},$$

and lattice parameters approximately

$$a = 0.4457 \text{ nm}, \qquad c = 0.5929 \text{ nm}$$

[Poborchii et al., 2022, Yi et al., 2018, Kirchhoff et al., 1994].

The predefined structural candidate set used in the exhaustive comparison was

$$\mathcal{L}_{\mathrm{Te}} = \left\{ r_h, \frac{c}{3}, \frac{a}{2}, d_{\mathrm{intra}}, d_{\mathrm{inter}}, a, c \right\},$$

where the helical radius is obtained from the intrachain bond and axial rise,

$$r_h = \sqrt{\frac{d_{\mathrm{intra}}^2 - (c/3)^2}{3}}.$$

This set was fixed before testing the ordered assignments.

Tellurium belongs to an enantiomorphic trigonal point group. The deposited chiral-point-group table distinguishes the axial magneto-chiral tensor coefficient from the equal transverse coefficients. This symmetry difference motivates separate axial and transverse compatibility channels but does not determine the structural assignment by itself.

4 QMU Formulation

4.1 Temperature

The QMU temperature unit is

$$\mathrm{temp} = {\lambda_C}^2 {F_q}^2.$$

The Kelvin bridge used in this analysis is

$$\theta(T) \equiv \frac{T}{\mathrm{temp}} = K_{\mathrm{cf}} T_{\mathrm{K}},$$

with

$$K_{\mathrm{cf}} = 3.3003306 \times 10^{-15}\ \frac{\mathrm{temp}}{\mathrm{K}}$$

from the QMU Ideal Gas Law treatment [Thomson III, 2024].

The main derivation uses θ as a dimensionless fraction of temp. Kelvin appears only as a bridge label for the deposited experimental temperature.

4.2 Frequency and resonance

A deposited terahertz frequency is converted by

$$\nu_n \equiv \frac{f_n}{\mathrm{freq}} = \frac{f_n}{F_q}.$$

The corresponding resonance is

$$r_n = \nu_n^2\,\mathrm{rson}.$$

4.3 Thermoresonant area and effective cross-section length

Since

$$\mathrm{temp} = \mathrm{area}\,\mathrm{rson},$$

the area associated with a measured temperature fraction and mode resonance is

$$A_n(T) = \frac{\theta(T)}{\nu_n^2}\,\mathrm{area}.$$

The corresponding effective thermoresonant cross-section length is

$$L_n(T) = \lambda_C \frac{\sqrt{\theta(T)}}{\nu_n},$$

with no adjustable scale factor.

The word *cross-section* identifies the origin of $L_n(T)$ in the temperature–area–resonance identity

$$\mathrm{temp} = \mathrm{area}\,\mathrm{rson}.$$

It does not imply that the crystal bond or lattice spacing physically expands to $L_n(T)$ as temperature changes.

The quantity $L_n(T)$ is therefore an effective resonant projection of the thermal area into a one-dimensional comparison scale. Structural registration occurs only at a condition for which this effective cross-section length equals a fixed crystal dimension:

$$L_n(T) = L_s.$$

4.4 Registration ratio

For a candidate structural length L_s, define

$$\boxed{\mathcal{R}_{n,s}(T) = \frac{L_n(T)}{L_s}}$$

and exact registration by

$$\mathcal{R}_{n,s} = 1.$$

4.5 Registration error and registration fidelity

For a three-branch ordered assignment Φ, the collective logarithmic registration error is

$$\mathcal{E}_{\mathrm{reg}}(T;\Phi) = \sqrt{\frac{1}{3}\sum_{n=1}^{3}\left[\ln \mathcal{R}_{n,s(n)}(T)\right]^2}.$$

For comparisons among independent datasets, it is useful to define the dimensionless structural-registration fidelity

$$\boxed{\mathcal{F}_{\mathrm{reg}} = \exp(-\mathcal{E}_{\mathrm{reg}})\,.}$$

This quantity satisfies

$$0 < \mathcal{F}_{\mathrm{reg}} \leq 1,$$

with

$$\mathcal{F}_{\mathrm{reg}} = 1$$

only for exact simultaneous registration.

The fidelity is a monotonic restatement of $\mathcal{E}_{\mathrm{reg}}$ and therefore introduces no additional evidence or fit parameter. Its purpose is to provide a bounded reporting scale for comparisons among future structural-registration analyses.

4.6 Compatibility rate

The deposited growth parameter is converted into the net compatibility rate

$$\boxed{\mathcal{K}_n = -2\pi\gamma_n}$$

with the same frequency dimension as f_n. Thus

$$\mathcal{K}_n > 0$$

denotes constructive amplification and

$$\mathcal{K}_n < 0$$

denotes decay.

5 Verified Numerical Results

5.1 Scale-independent ratio test

Before introducing the absolute QMU compatibility lengths, the relative geometric structure of the spectrum can be tested directly from the deposited frequencies. This is the most model-independent component of the analysis because it does not require the Kelvin-to-temp conversion or any absolute QMU scale.

The relation

$$L_n \propto \frac{1}{f_n}$$

at fixed temperature implies

$$\frac{f_i}{f_j} \approx \frac{L_j}{L_i}.$$

This ratio test cancels K_{cf}, λ_C, and F_q. It therefore tests the ordering and relative spacing without relying on the Kelvin-to-temp bridge.

Using the core branch as the reference, the low/core and high/core ratio residuals are approximately 2.64% and 2.23%, respectively.

The ratio test therefore establishes that the ordered spectral spacing already approximates the inverse ordering of the proposed structural dimensions before the absolute QMU temperature conversion is applied. The absolute registration test that follows determines whether the common scale also agrees.

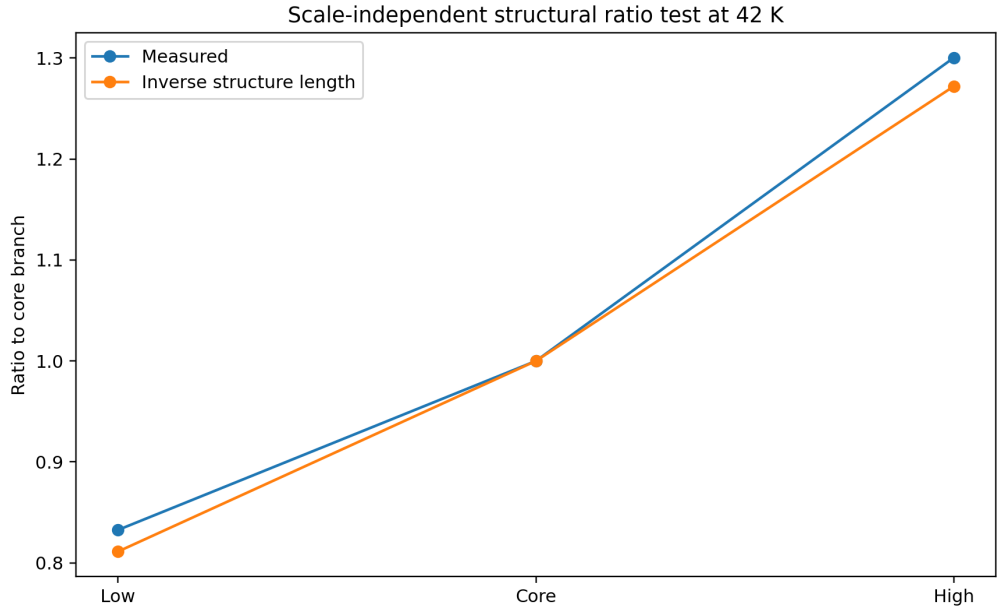

Figure 1: Measured frequency ratios compared with inverse assigned-structure ratios at the 42 K condition. This test is independent of the absolute QMU temperature conversion.

5.2 Hierarchy of evidentiary dependence

The analysis contains results with different levels of dependence on the QMU conversion bridge.

The following results are determined directly from the deposited mode frequencies and the predefined structural candidate set:

1. the ordering of the low, core, and high branches;
2. the inverse ordering of the assigned structural dimensions;
3. the scale-independent frequency-ratio residuals;
4. the finite combinatorial structure of the assignment problem; and
5. the relative assignment ordering once a common absolute scale is supplied.

The identity of the absolute minimum-error assignment and its localization in the deposited temperature series depend on the common scale supplied by the Kelvin-to-temp bridge.

Accordingly, the paper does not rest on one conversion-dependent observation. It combines a relative geometric test with an absolute QMU registration test. The two tests examine different parts of the same proposed mapping.

5.3 Unique registration at the deposited 42 K condition

The principal numerical discovery is an optimal structural assignment, not merely a visual resemblance between three numbers. At the deposited 42 K condition, the complete 210-assignment search identifies one ordered mapping with the minimum collective registration error:

$$\Phi_{\min}(42\,\mathrm{K}) = \left(d_{\mathrm{inter}}, d_{\mathrm{intra}}, \frac{a}{2}\right).$$

At the temperature labeled 42 K in the SI bridge, the deposited transverse branches are

$$f_{\mathrm{low}} = 0.326099\ \mathrm{THz},$$

$$f_{\mathrm{core}} = 0.391682\ \mathrm{THz},$$

and

$$f_{\mathrm{high}} = 0.509383\ \mathrm{THz}.$$

Their QMU thermoresonant lengths obtained from Eq. (4.3) are

$$L_{\mathrm{low}} = 0.342274\ \mathrm{nm},$$

$$L_{\mathrm{core}} = 0.284964\ \mathrm{nm},$$

and

$$L_{\mathrm{high}} = 0.219119\ \mathrm{nm}.$$

The optimum assignment is

$$\boxed{L_{\mathrm{low}} \leftrightarrow d_{\mathrm{inter}}, \qquad L_{\mathrm{core}} \leftrightarrow d_{\mathrm{intra}}, \qquad L_{\mathrm{high}} \leftrightarrow \frac{a}{2}}$$

with fractional mismatches

$$-2.07\%, \qquad +0.52\%, \qquad -1.68\%.$$

Table 1: Three-mode structural registration at the deposited 42 K condition.

Branch	f_n (THz)	L_n (nm)	Assigned structure (nm)	Mismatch
Low	0.326099	0.342274	0.349500	-2.07%
Core	0.391682	0.284964	0.283500	$+0.52\%$
High	0.509383	0.219119	0.222850	-1.68%

The collective error is

$$\boxed{\mathcal{E}_{\mathrm{reg}}(42\,\mathrm{K}) = 0.015791}$$

and the root-mean-square fractional length mismatch is

$$\boxed{1.5646\%.}$$

The corresponding structural-registration fidelity is

$$\mathcal{F}_{\mathrm{reg}}(42\,\mathrm{K}) = \exp(-0.015791) = 0.98433.$$

This bounded value is provided for comparison with future applications. The optimization and assignment ranking continue to use $\mathcal{E}_{\mathrm{reg}}$, not its monotonic fidelity transform.

The next-best assignment has

$$\mathcal{E}_{\mathrm{reg}} = 0.060864,$$

which is approximately

$$3.86$$

times larger than the optimum error. The optimum is therefore separated substantially from the nearest competing assignment within the predefined search space.

For comparison, the next-best assignment has

$$\mathcal{F}_{\mathrm{reg},2} = \exp(-0.060864) \approx 0.94095.$$

The distinction between the two assignments is assessed through their registration errors and assignment rank; the fidelity values provide a compact secondary reporting scale.

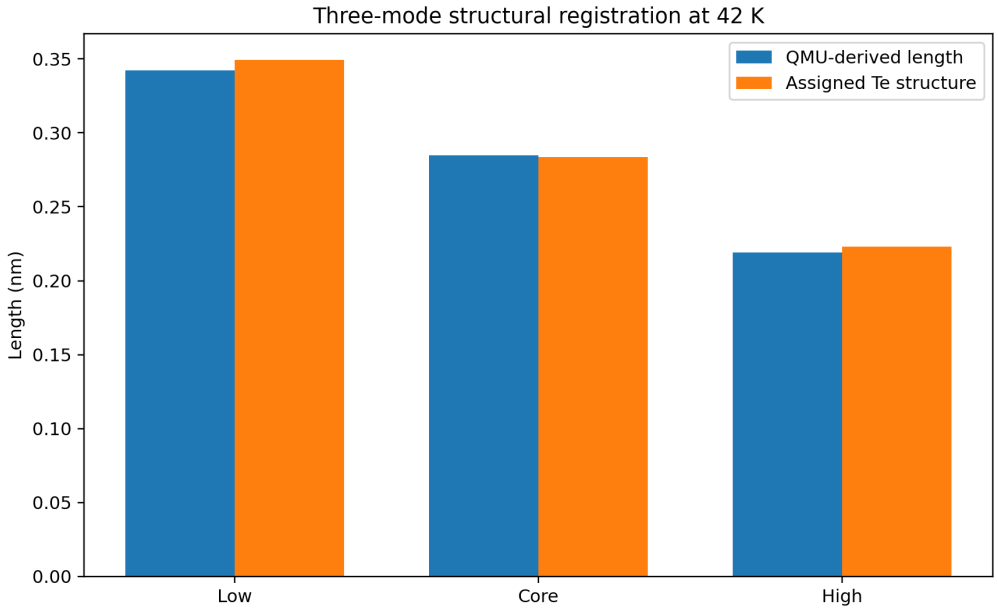

Figure 2: QMU-derived thermoresonant lengths compared with the three assigned tellurium structures at the deposited 42 K condition.

5.4 Exhaustive assignment test

Seven predefined structural lengths yield

$$7 \times 6 \times 5 = 210$$

ordered three-length assignments. Every assignment was tested using Eq. (4.5). The assignment in Eq. (5.3) ranks first at 42 K. The second-best assignment gives

$$\mathcal{E}_{\mathrm{reg}} = 0.060864,$$

which is approximately 3.86 times larger than the optimum error.

This result is important because the three structures were not independently selected after calculating each effective length. They were compared as one ordered triplet against the complete predefined candidate set.

5.5 Deterministic frequency-sensitivity test

The deposited oscillator files do not provide covariance matrices. A formal uncertainty propagation is therefore unavailable. The stability of the optimum assignment can nevertheless be tested deterministically by perturbing the three deposited frequencies.

Let

$$f_n' = f_n + \delta f_n,$$

with independently bounded perturbations

$$|\delta f_n| \leq \Delta f.$$

For every perturbed frequency triplet, the effective cross-section lengths and all 210 ordered assignment errors are recalculated. Define the assignment robustness radius by

$$\Delta f_{\mathrm{rob}} = \inf \left\{ \Delta f : \exists \, (\delta f_{\mathrm{low}}, \delta f_{\mathrm{core}}, \delta f_{\mathrm{high}}) \text{ such that } \Phi'_{\mathrm{min}} \neq \Phi_{\mathrm{min}} \right\}.$$

A bounded adversarial search gives

$$\boxed{\Delta f_{\mathrm{rob}} \approx 0.02247\,\mathrm{THz} = 22.47\,\mathrm{GHz}.}$$

The first competing assignment to reach equal error is

$$\left(d_{\mathrm{inter}}, d_{\mathrm{intra}}, \frac{c}{3} \right),$$

which replaces the high-branch assignment $a/2$ with the axial rise $c/3$.

The boundary is approached by coordinated shifts of approximately One minimum-bound adversarial solution approaches the assignment boundary with

$$\delta f_{\mathrm{low}} \approx -6.76\,\mathrm{GHz},$$

$$\delta f_{\mathrm{core}} \approx +2.01\,\mathrm{GHz},$$

and

$$\delta f_{\mathrm{high}} \approx +22.47\,\mathrm{GHz}.$$

The high branch therefore controls the first assignment change in this bounded search.

Thus, within the fixed candidate set and fixed QMU bridge, no independent three-frequency perturbation bounded below approximately 22 GHz changes the identity of the optimum assignment.

This is a deterministic robustness result, not a confidence interval. It does not substitute for fit covariance or raw-trace refitting, but it quantifies how far the deposited best-fit spectrum must move before the first-rank assignment is lost.

5.6 Temperature localization

Table 2 gives the error of the proposed assignment across the full deposited transverse-temperature series.

Table 2: Registration of the 42 K structural assignment across the deposited temperature series.

Bridge temperature	$\mathcal{E}_{\mathrm{reg}}$	RMS mismatch	Assignment rank	Amplified branches
12	0.641495	47.35%	47	3
42	0.015791	1.56%	1	3
80	0.327588	38.77%	25	3
120	0.523368	68.78%	47	3
160	0.633863	88.49%	56	2
200	0.718361	105.23%	58	2

The proposed assignment is therefore not a permanent identity of the three branches. It is a sharply localized thermoresonant compatibility window. The earlier possibility that the same assignment remained optimal at all temperatures is rejected by the exhaustive computation.

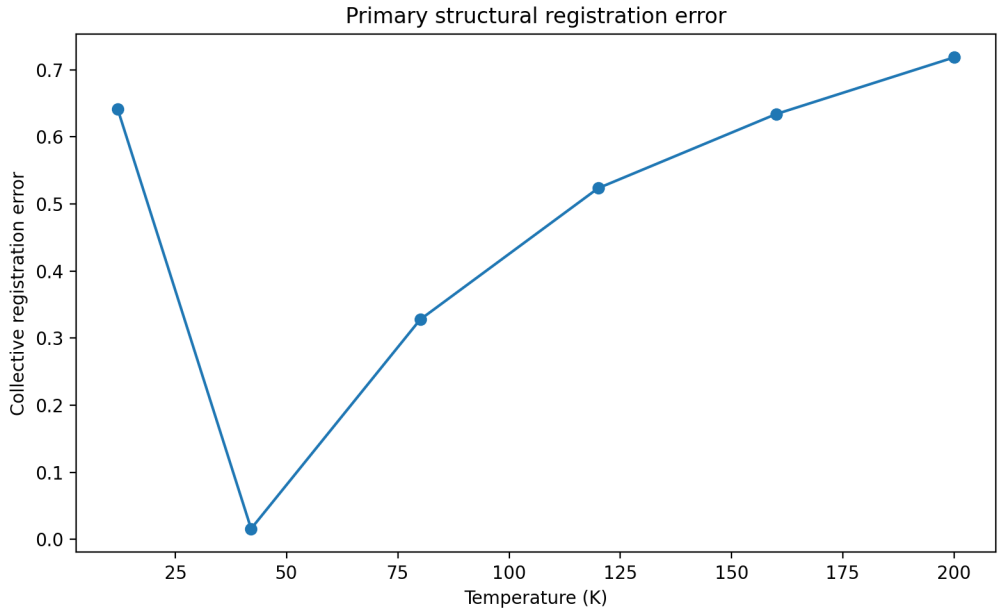

Figure 3: Collective registration error of the proposed structural assignment across the deposited transverse-temperature series. The 42 K condition is the unique minimum.

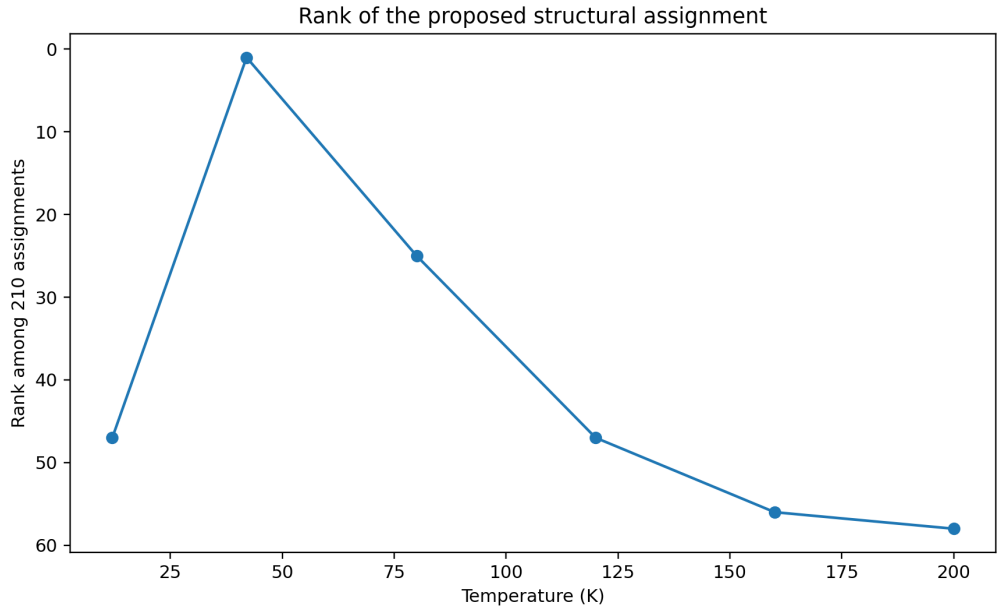

Figure 4: Rank of the proposed assignment among all 210 ordered structural assignments. It ranks first only at the 42 K condition.

5.7 Structural-match temperatures

For a fixed structure L_s and measured frequency f_n, exact registration determines a structural-match temperature

$$\boxed{T_{s,n} = \frac{1}{K_{\mathrm{cf}}} \left(\frac{L_s f_n}{c} \right)^2}$$

where SI symbols occur only in the bridge evaluation.

At the 42 K spectrum, the three inferred values are approximately

$$T_{\mathrm{low}} = 43.79 \text{ K},$$

$$T_{\mathrm{core}} = 41.57 \text{ K},$$

and

$$T_{\mathrm{high}} = 43.45 \text{ K}.$$

Their mean and sample standard deviation are

$$\boxed{T_{\mathrm{reg}} = 42.9347 \pm 1.1951 \text{ K}.}$$

This convergence is independent across three measured modes and three structural dimensions.

6 Compatibility Landscape

6.1 Orientation-dependent branch availability

The deposited field scans show a qualitative difference between the axial and transverse orientations. The axial geometry supports one persistent amplified core branch near the middle of the transverse spectrum, whereas the transverse geometry supports three distinguishable amplified branches over the low-temperature range.

This can be represented by a branch selector

$$S_n(\vartheta),$$

where ϑ is the angle between the applied magnetic flux density and the crystal c-axis. At the two measured limits,

$$S_{\mathrm{core}}(0) = 1,$$

while

$$S_{\mathrm{low}}(0) \approx 0, \qquad S_{\mathrm{high}}(0) \approx 0,$$

and

$$S_{\mathrm{low}}\left(\frac{\pi}{2}\right) = S_{\mathrm{core}}\left(\frac{\pi}{2}\right) = S_{\mathrm{high}}\left(\frac{\pi}{2}\right) = 1.$$

The full angular selector remains unmeasured.

6.2 Growth relative to structural registration

The verified assignment result and the measured amplification rate are distinct observables. Structural registration is obtained from the relation among temperature, frequency, and fixed crystal dimensions. Amplification is obtained from the fitted exponential coefficient. The two should not be conflated.

A useful phenomenological decomposition of the measured net compatibility rate is

$$\mathcal{K}_n(T, B, \vartheta) = G_n(T, B, \vartheta) - D_n(T, B, \vartheta),$$

where G_n is constructive drive and D_n is dissipation. Structural registration is proposed to enhance G_n, but the measured rate remains the difference of both terms.

The deposited rates generally weaken as the proposed structural mismatch increases, especially for the core branch. However, the sparse temperature sampling and absence of deposited parameter covariance prevent a formal causal claim.

The verified result is therefore the minimum-error structural assignment. The proposal that structural registration enhances the constructive drive G_n is an APM interpretation and a target for future experiment.

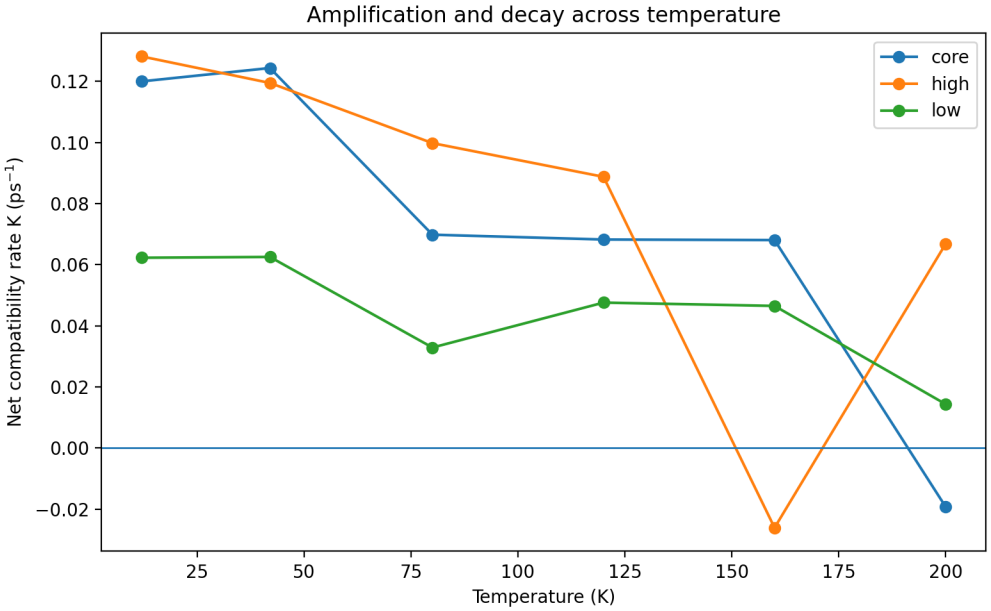

Figure 5: Net compatibility rates of the three transverse branches. Positive values denote amplification under the deposited fitting convention.

7 Constructive Interpretation

7.1 Three levels of result

The findings of this paper should be distinguished at three levels.

Level I: numerical result. The deposited 42 K spectrum possesses a unique minimum-error ordered assignment within the complete predefined 210-assignment search space.

Level II: geometric result. The optimum assignment maps the three measured branches onto three distinct dimensions of the trigonal tellurium structure with an RMS fractional mismatch of 1.5646%, while the independent frequency-ratio test agrees at the few-percent level.

Level III: APM interpretation. The localized assignment is interpreted as a thermoresonant compatibility window within which three oscillatory pathways register simultaneously with the stable crystal geometry. The term *window* refers to the localization of the optimum assignment in the thermal control variable. It does not imply that the deposited six-point series has already resolved the width or detailed profile of that window.

The first level is purely computational. The second identifies an ordered geometric organization. The third supplies the constructive physical interpretation. Failure of the APM interpretation would not erase the verified numerical assignment, but successful experimental predictions would strengthen the interpretation.

7.2 A localized thermoresonant compatibility window

The verified result is most naturally expressed as a localized compatibility window:

$$\boxed{\text{three resonant pathways} \longleftrightarrow \text{three fixed lattice dimensions}}$$

at one localized thermal condition. In the APM interpretation, the crystal does not acquire its structural dimensions from the external field. The dimensions already exist as stable matter geometry. Photoexcitation provides available energy, the magnetic orientation selects accessible pathways, and the temperature–resonance relation determines whether the active oscillatory geometry registers with the crystal.

The constructive sequence is

$$\begin{aligned} \text{helical crystal geometry} &\longrightarrow \text{allowed resonant branches} \\ &\longrightarrow \text{magnetic orientation selection} \\ &\longrightarrow \text{thermoresonant registration} \\ &\longrightarrow \text{coherent growth or decay.} \end{aligned}$$

7.3 Structural meaning of the three branches

The optimum assignment suggests the following preliminary interpretation:

- the low branch corresponds to interchain compatibility;
- the core branch corresponds to intrachain helical compatibility;
- the high branch corresponds to a transverse half-cell pathway.

The core branch is the strongest individual match and appears in both axial and transverse orientations. This makes the intrachain Te–Te bond the most plausible geometric anchor of the common branch.

The low and high branches become prominent in the transverse orientation, which is consistent with their association with interchain and transverse-cell geometry. This is an interpretation of the verified ordering, not a direct imaging of the oscillatory displacement pattern.

7.4 Why the registration is localized

Equation (4.3) gives

$$L_n(T) \propto \frac{\sqrt{T/\mathrm{temp}}}{f_n(T)/\mathrm{freq}}.$$

Because the deposited frequencies shift much less than $\sqrt{T}$, the effective compatibility lengths generally expand with temperature. The fixed crystal dimensions are therefore crossed simultaneously only within a limited thermoresonant compatibility window.

The result should not be stated as "the QMU mode length equals the bond length." The accurate statement is:

> The QMU thermoresonant compatibility lengths of the three transverse branches simultaneously equal three fixed tellurium dimensions within approximately 1.6% RMS at the deposited 42 K condition, and the assignment is the optimum among the complete predefined comparison set.

8 Alternative Explanations and Evidentiary Limits

8.1 No propagated oscillator uncertainties

The deposited parameter files contain fitted values but not fit covariance matrices. The analysis therefore cannot assign a formal significance to the 1.5646% mismatch. Raw-trace refitting or author-supplied parameter uncertainties would permit Monte Carlo propagation through Eqs. (4.3)–(4.5).

Section 5.5 provides a complementary deterministic sensitivity test. That test shows that the optimum assignment survives all independently bounded frequency perturbations below approximately 22.5 GHz within the defined structural candidate set. This robustness radius measures assignment stability but must not be interpreted as an experimental standard deviation.

8.2 Conversion-factor dependence

The absolute length registration depends on K_{cf}. The scale-independent ratio test does not. Agreement of both tests is stronger than either alone, but an independent refinement of the Kelvin-to-temp bridge would shift all absolute match temperatures.

8.3 Look-elsewhere structure

The exhaustive assignment test controls the ordering within the predefined seven-length candidate set. It does not eliminate every conceivable derived crystal length. For that reason, the paper reports the candidate set explicitly and does not enlarge it after seeing the optimum.

8.4 One dataset

The result is obtained from one published sample and one deposited analysis. Independent tellurium crystals, opposite enantiomorphs, varied strain, varied pressure, or isotope substitution are required to establish a repeatable structural law.

8.5 Assignment is not yet identification

The numerical optimum establishes that one structural assignment minimizes the defined registration error within the stated candidate set. It does not by itself prove that the corresponding atomic displacements have been directly observed.

The branch labels

interchain, intrachain, transverse half-cell

are therefore proposed geometric assignments. Direct mode imaging, lattice dynamics calculations, pressure dependence, or strain-selective frequency shifts are required to convert the numerical assignment into a physical mode identification.

8.6 No claim of microscopic exclusivity

The present result does not refute the authors' polariton and magneto-chiral conductivity treatment. It identifies an additional numerical organization in the deposited spectrum. The measured registration can be incorporated into, compared with, or distinguished from other descriptions through future experiments.

9 Predictions

The structural-registration hypothesis produces direct tests.

9.1 Pressure and strain

If a branch is tied to a structural length L_s, then at fixed QMU temperature

$$f_n \propto \frac{1}{L_s}.$$

For a small deformation,

$$\boxed{\frac{\Delta f_n}{f_n} \approx -\frac{\Delta L_s}{L_s}}$$

with different shifts expected for interchain, intrachain, and transverse-cell deformation.

9.2 Branch-specific assignment test

The proposed mapping predicts distinct responses because the assigned structural dimensions do not deform identically.

A perturbation that predominantly changes the interchain separation should produce its largest relative shift in the low branch. A perturbation that modifies the intrachain Te–Te bond should most strongly affect the core branch. A transverse lattice deformation should preferentially shift the high branch.

The assignment is therefore falsified if the measured branch shifts do not follow the ordering

$$\left|\frac{\Delta f_{\mathrm{low}}}{f_{\mathrm{low}}}\right| : \left|\frac{\Delta f_{\mathrm{core}}}{f_{\mathrm{core}}}\right| : \left|\frac{\Delta f_{\mathrm{high}}}{f_{\mathrm{high}}}\right|$$

expected from the independently measured changes in

$$d_{\mathrm{inter}}, \qquad d_{\mathrm{intra}}, \qquad \frac{a}{2}.$$

9.3 Angular scan

Rotating the magnetic field continuously from $B \parallel c$ to $B \perp c$ should reveal the opening of the low and high structural branches. The branch amplitudes and growth rates should provide the missing angular selector $S_n(\vartheta)$.

9.4 Opposite crystal handedness

Reversing the crystal enantiomorph should reverse the field-odd emitted orientation while preserving the structural frequencies and the magnitude of the registration condition:

$$f_n(-\chi) = f_n(\chi),$$

$$\mathcal{E}_{\mathrm{reg}}(-\chi) = \mathcal{E}_{\mathrm{reg}}(\chi),$$

but

$$E_{\mathrm{odd}}(-\chi) = -E_{\mathrm{odd}}(\chi).$$

9.5 Temperature refinement

A dense scan from approximately 35 to 50 K should determine whether the collective error minimum and the compatibility-rate maximum coincide. The present six-point temperature series establishes localization but not the detailed shape of the registration basin.

9.6 Independent structural perturbation

Substitution, isotope variation, or controlled lattice modification should shift the three branches according to their assigned geometric channels. A common unexplained shift would weaken the branch-specific assignment; differential shifts consistent with Eq. (9.1) would strongly support it.

10 Discussion

The verified computation reveals a result that is difficult to see in the original SI variables. Temperature is given in kelvin, frequency in terahertz, and structure in nanometres. The QMU identity

$$\text{temp} = \text{area}\,\text{rson}$$

places these quantities into one dimensional ledger. Once temperature and resonance are combined, the three-mode spectrum becomes a set of effective areas and lengths that can be compared directly with the crystal.

The result is not a generic consequence of increasing temperature. The proposed assignment ranks first only at the 42 K condition and falls far down the assignment list at every other measured temperature. This is precisely the behavior expected of a compatibility window: the minimum-error assignment appears within a localized thermal interval rather than remaining trivially optimal everywhere.

The strongest part of the discovery is the combination of four tests:

1. three modes register simultaneously rather than one mode matching one number;
2. the ordered assignment is the optimum among 210 predefined alternatives;
3. the inferred structural-match temperatures converge near 42.9 K; and
4. the scale-independent frequency ratios agree with inverse structural ratios.

The weakest part is the absence of deposited fit uncertainties and independent replication. The appropriate scientific posture is therefore neither dismissal nor overstatement.

The result is more precisely described as a reproducible minimum-error structural assignment rather than as a generic numerical correlation. Its physical significance remains to be determined experimentally, but the assignment is explicit, finite, reproducible, and associated with distinct predictions.

A general QMU structural-registration method

The tellurium analysis also defines a reusable procedure for other systems:

1. obtain a deposited experimental spectrum;
2. identify branches using the original authors' analysis rather than a QMU-optimized selection;
3. convert the measured observables into QMU temperature, frequency, resonance, area, and effective cross-section length;
4. define a structural candidate set before evaluating the spectrum;

5. solve the complete ordered assignment problem;
6. calculate the minimum registration error, registration fidelity, and separation from the next-best assignment;
7. perform a scale-independent ratio test;
8. calculate a deterministic perturbation radius for assignment stability;
9. propagate experimental covariance when it is available; and
10. formulate structural perturbations that distinguish the proposed assignments.

This procedure defines a reusable QMU structural-registration methodology applicable to independent crystal, molecular, magnetic, and particle spectra. The combination of a predefined candidate basis, exhaustive assignment, conversion-independent ratio testing, and perturbation stability is intended to prevent a visually suggestive numerical match from being treated as a structural result without adequate controls. Repeated success across unrelated systems would establish QMU structural registration as a general analytical method. Failure to produce stable or predictive assignments would limit its scope.

11 Conclusion

A complete reanalysis of the deposited transverse-temperature oscillator parameters for photoexcited tellurium has been performed as a finite structural assignment problem in QMU.

The analysis defines the effective thermoresonant cross-section length

$$L_n(T) = \lambda_C \frac{\sqrt{T/\mathrm{temp}}}{f_n/\mathrm{freq}},$$

constructs a predefined seven-length tellurium candidate set, and evaluates all

$$7 \times 6 \times 5 = 210$$

ordered assignments for the three amplified transverse branches.

At the deposited 42 K condition, the low, core, and high branches register respectively with the interchain separation, intrachain bond, and transverse half-cell dimension. The collective logarithmic error is

$$\mathcal{E}_{\mathrm{reg}} = 0.015791,$$

corresponding to an RMS mismatch of

$$1.5646\%.$$

The assignment is the unique optimum among all 210 ordered assignments from the predefined structural set. The three inferred exact-match temperatures converge at

$$T_{\mathrm{reg}} = 42.9347 \pm 1.1951 \text{ K},$$

and a conversion-independent ratio test agrees at the few-percent level.

The ratio test establishes the relative geometric ordering independently of the Kelvin-to-temp bridge, while the absolute QMU registration establishes the common scale and localized match temperature.

Together, these results identify an optimal structural mapping rather than a single isolated numerical coincidence.

The same assignment is not optimal at the other deposited temperatures. The verified claim is therefore a localized thermoresonant compatibility window:

> The deposited transverse magneto-chiral spectrum of tellurium exhibits a unique minimum-error three-mode structural assignment near 42 K, interpreted in the APM as a localized thermoresonant compatibility condition.

Beyond the tellurium application, the analysis establishes a general computational method:

deposited spectrum ⟶ predefined geometric basis ⟶ exhaustive assignment ⟶ ratio validation ⟶ robustness

The method is not validated as universal by one material. Its value will be determined by whether the same predefined and reproducible procedure yields stable, perturbation-resistant, and experimentally predictive assignments in independent systems.

The next decisive experiments are a dense temperature scan across the proposed compatibility window, a continuous magnetic-angle scan, and controlled structural perturbations. These tests can determine whether the observed registration is a reproducible property of chiral tellurium or a numerical coincidence in the present dataset.

A SI-to-QMU Bridge

The main text is QMU-first. This appendix records the SI values required to reproduce the deposited-data conversion.

A.1 Base bridge values

The values used are

$$\lambda_C = 2.42631023538 \times 10^{-12}\ \mathrm{m},$$
$$F_q = \frac{c}{\lambda_C} = 1.235589965 \times 10^{20}\ \mathrm{s}^{-1},$$

and

$$K_{\mathrm{cf}} = 3.3003306 \times 10^{-15}\ \frac{\mathrm{temp}}{\mathrm{K}}.$$

The first two are based on CODATA bridge values [Tiesinga et al., 2023]; the temperature factor follows the cited QMU thermal treatment [Thomson III, 2024].

A.2 Frequency

A frequency quoted in terahertz is converted by

$$\frac{f}{\mathrm{freq}} = \frac{f_{\mathrm{THz}} \times 10^{12}}{F_q}.$$

A.3 Temperature

A temperature quoted in kelvin is converted by

$$\frac{T}{\text{temp}} = K_{\text{cf}} T_{\text{K}}.$$

A.4 Magnetic flux density

The present structural-registration calculation does not use the magnetic-field magnitude as an independent variable. Where magnetic flux density is converted in future extensions, the tesla-to-mfxd bridge must include the electron-sector charge conversion factor rather than applying a purely dimensional rescaling [Thomson III, 2025b].

B Complete Registration Table

Table 3: Primary structural assignment across the deposited transverse-temperature series.

T (K)	Branch	f (THz)	Assigned structure	L_{eff} (nm)	Mismatch
12	low	0.3258	interchain	0.1828	−47.7%
12	core	0.3946	intrachain	0.1510	−46.7%
12	high	0.5100	$a/2$	0.1168	−47.6%
42	low	0.326099	interchain	0.342274	−2.07%
42	core	0.391682	intrachain	0.284964	+0.52%
42	high	0.509383	$a/2$	0.219119	−1.68%
80	low	0.3225	interchain	0.4778	+36.7%
80	core	0.3900	intrachain	0.3952	+39.4%
80	high	0.4934	$a/2$	0.3123	+40.1%
120	low	0.3217	interchain	0.5867	+67.9%
120	core	0.3907	intrachain	0.4831	+70.4%
120	high	0.5041	$a/2$	0.3744	+68.0%
160	low	0.3334	interchain	0.6538	+87.1%
160	core	0.4076	intrachain	0.5348	+88.6%
160	high	0.5154	$a/2$	0.4229	+89.8%
200	low	0.3366	interchain	0.7243	+107.2%
200	core	0.4080	intrachain	0.5976	+110.8%
200	high	0.5548	$a/2$	0.4394	+97.2%

C Analysis Algorithm

The verified computation follows this sequence:

1. read the deposited MATLAB parameter files;
2. select deposited modes 4–6 for the transverse-temperature spectrum;

3. convert T to T/temp;
4. convert f_n to f_n/freq;
5. calculate $L_n(T)$ from Eq. (4.3);
6. evaluate all 210 ordered assignments from $\mathcal{L}_{\mathrm{Te}}$;
7. rank assignments by Eq. (4.5);
8. perturb the three deposited frequencies independently within a common bounded interval and re-evaluate all 210 assignments;
9. determine the smallest perturbation bound at which the first-rank assignment changes;
10. calculate exact structural-match temperatures;
11. perform the conversion-independent frequency-ratio test; and
12. export every table and figure used in the manuscript.

The assignment-robustness calculation minimizes the error difference between the primary assignment and every competing assignment subject to

$$|\delta f_n| \leq \Delta f.$$

The smallest bound for which a competitor attains equal or lower error is reported as Δf_{rob}. The calculation is deterministic and does not assume a probability distribution for the unavailable fit uncertainties.

Data and Code Availability

The source experimental data and deposited analysis are available from the Illinois Data Bank under DOI 10.13012/B2IDB-1409842_V3. The derived tables and reproduction script accompanying this paper are transformations of that archive. The experimental data are CC BY 4.0 and the source analysis code is MIT licensed [Huang and Abboud, 2025].

Acknowledgments

The Quantum AetherDynamics Institute is a private 501(c)(3) research institute developing the Aether Physics Model and Quantum Measurement Units [Thomson III, 2025a]. The author acknowledges Yijing Huang, Nick Abboud, and their collaborators for publishing a detailed and reusable experimental archive.

References

Yijing Huang and Nick Abboud. Data for observation of a dynamic magneto-chiral instability in photoexcited tellurium. Illinois Data Bank, 2025. URL https://doi.org/10.13012/B2IDB-1409842_V3. Data files under CC BY 4.0; deposited analysis code under the MIT License.

Yijing Huang, Nick Abboud, Yinchuan Lv, Penghao Zhu, Azel Murzabekova, Changjun Lee, Emma A. Pappas, Dominic Petruzzi, Jason Y. Yan, Dipanjan Chaudhuri, Peter Abbamonte,

Daniel P. Shoemaker, Rafael M. Fernandes, Jorge Noronha, and Fahad Mahmood. Dynamic magneto-chiral instability in photoexcited tellurium. *Nature Physics*, 22:202–208, 2026. doi: 10.1038/s41567-025-03145-8. URL https://doi.org/10.1038/s41567-025-03145-8.

F. Kirchhoff et al. Structural and bonding properties of solid tellurium from first principles. *Physical Review B*, 50:9063–9070, 1994. doi: 10.1103/PhysRevB.50.9063. URL https://doi.org/10.1103/PhysRevB.50.9063.

Vladimir V. Poborchii et al. Optical properties of extreme tellurium nanowires formed in channels of alpo4-5 single crystals. *Scientific Reports*, 12:21694, 2022. doi: 10.1038/s41598-022-26158-0. URL https://doi.org/10.1038/s41598-022-26158-0.

David W. Thomson III. A novel interpretation of the ideal gas law and its relation to black body radiation using the aether physics model, October 2024. URL https://doi.org/10.13140/RG.2.2.30228.31368. Licensed under CC BY-ND 4.0.

David W. Thomson III. Quantum aetherdynamics institute (QADI): Community DOI overview and citation guide. Zenodo, 2025a. URL https://doi.org/10.5281/zenodo.17479314.

David W. Thomson III. The charge conversion factor in the aether physics model: From singular to distributed charge, with rules, exceptions, and benchmarks. Zenodo, 2025b. URL https://doi.org/10.5281/zenodo.17451188.

David W. Thomson III. Reference tables for quantum measurement unit (QMU) conversions: CGS and MKS systems. Zenodo, 2025c. URL https://doi.org/10.5281/zenodo.17683574.

E. Tiesinga, P. J. Mohr, D. B. Newell, and B. N. Taylor. CODATA recommended values of the fundamental physical constants: 2022. *Reviews of Modern Physics*, 95:025010, 2023. doi: 10.1103/RevModPhys.95.025010. URL https://doi.org/10.1103/RevModPhys.95.025010.

Shuang Yi et al. The nature of bonding in bulk tellurium composed of one-dimensional helical chains. *Inorganic Chemistry*, 57:5083–5090, 2018. doi: 10.1021/acs.inorgchem.7b03244. URL https://doi.org/10.1021/acs.inorgchem.7b03244.